Supplementary Material for:

Active touch sensing in the rat: Anticipatory and regulatory control of whisker movements during surface exploration

Robyn A. Grant, Ben Mitchinson, Charles W. Fox, and Tony J. Prescott
Department of Psychology, University of Sheffield, UK

Contents

1 Supplementary Methods

1.1 Recording apparatus and 2D tracking methods

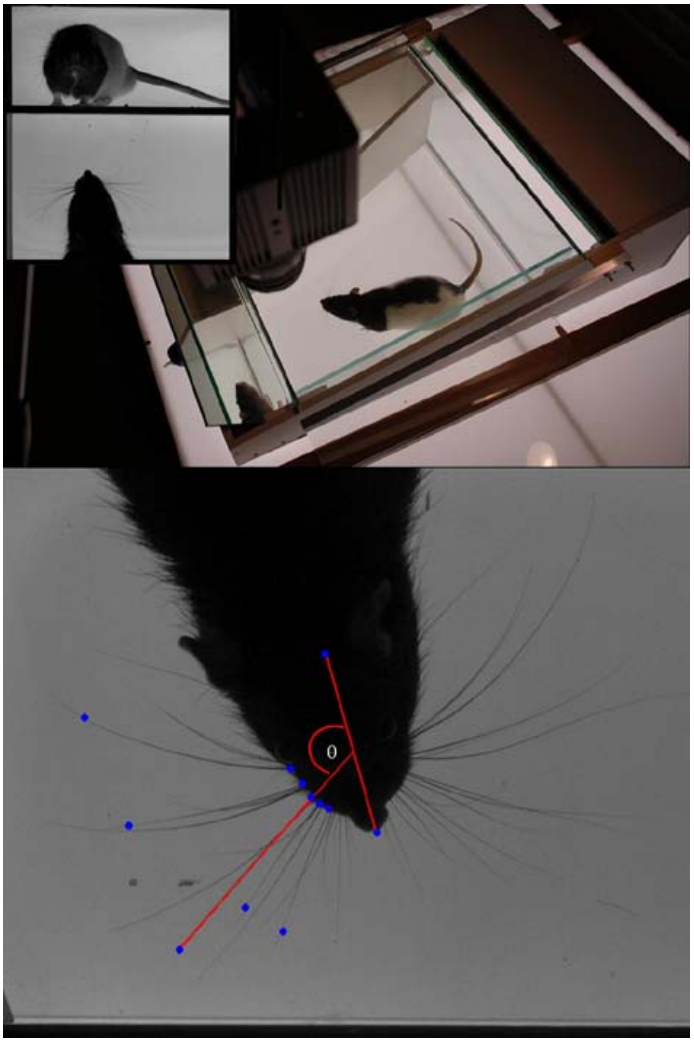

Figure S1. Recording and tracking methods. *Top:* The high-speed camera was positioned above a purpose-built viewing arena illuminated by a light-box. 3-4s recordings are captured opportunistically, and in two viewing planes (horizontal and vertical) whenever the animal enters a 20x20x8 cm viewing area. The inset shows the camera view. *Bottom:* Screen-shot showing tracked points (blue) and oriented lines (red) indicating how whisker angular positions were estimated in each frame. Note that the angular position of each tracked whisker (θ) is defined in a head-based co-ordinate frame.

Arena calibration

At the beginning of each filming session the camera was positioned on the z-axis (approximately 500millimetres above the floor plane), and the mirror aligned manually, so that the top-down and side-on view (via the mirror) were looking directly along the z-/y-axis (see Figure S1). A calibration shot was then taken of a specialized calibration tool, located at a known position in the arena. From the recorded footage, a calibration program allowed the tracker to identify seven localizable points of the tool, which were then used to calibrate the camera model (Tsai, 1987) using linear optimization. All clips belonging to that session would thus be pre-calibrated.

2D whisker tracking

Five whiskers, ipsilateral to the initial contact, were tracked on an LCD flat-screen monitor by a human observer using uncompressed video and a purpose-built tracking tool. Whisker tracking used only the overhead view and involved tracking two points, one near the base of the whisker [x1, y1], the other 2/3s of the way out along the whisker shaft [x2, y2] (see Figure S1). In each frame, the angular position, θ, of each whisker was calculated by (i) taking vector from [x1, y1] (base) to [x2, y2] (shaft); (ii) computing the angle of that vector in x/y space, (iii) offsetting that angle by the head bearing to obtain the head-centric angle.

Tracking error

Since tracking was performed by a single observer we used spectral analysis to calculate an estimate of tracking error as follows.

We expect the recorded position, *R(n)*, of a target object (e.g. a point on the whisker shaft) to be equal to its true position plus some uncorrelated tracking error, $R(n)=T(n)+E(n)$. Since *T(n)* is unavailable (we have no independent measure of the whisker position), we cannot obtain *E(n)* directly. However, *T(n)* will have power only in the range of frequencies at which the target actually moves. Whilst there may be movement of the whiskers above whisking frequencies, we expect that this power will, nonetheless, be largely confined to the low-end of the spectrum (below some frequency, f_T). In contrast, *E(n)* will be flat spectrum. Thus, we can approximately separate *E(n)* and *T(n)* by frequency band.

High-pass filtering *R(n)* with a cutoff frequency of f_C and measuring the power obtains the power in $T(n)+E(n)$ above f_C. With $f_C<f_T$, we expect contributions from both *T(n)* and *E(n)*; conversely, with $f_C>f_T$, we expect a contribution only from *E(n)*, and thus we obtain an estimate of the power in the error signal in the high band between f_C and the Nyquist frequency, f_N. Multiplying by $f_N/(f_N-f_C)$ recovers an estimate of the total power in the flat-spectrum error signal. Thus, we expect this calculated estimate to fall as we increase f_C towards f_T, and level out to remain fairly constant as f_C ranges between f_T and f_N (note that we do not know f_T *a priori*).

For our 2D tracking data we used this approach to assess the error in two classes of time series.

First, we obtained an estimate of the error magnitude in the raw tracking data, i.e. sequences of tracked points [x2, y2] corresponding to positions on the whisker shaft. As f_C increases, the estimate drops as expected, leveling out above about 70Hz. With f_C between 70 and 110Hz (f_N=125Hz), the resulting variance estimate varies by not more than 10%, and corresponds to a standard error (i.e. standard deviation of the error) of around 2.5 pixels.

Second, because our main analysis is concerned only with the angular position of the whisker, we calculated a second estimate of the error magnitude based on the whisker angle data (θ). As expected, the estimate of f_T again levels out above 70Hz, from which we estimate the standard error in the whisker angle data (θ) as 0.25 degrees. Reversing the geometric transforms that were applied to compute θ, we find that the error in the tracked positions perpendicular to the whisker shift is around 1.2 pixels. This value is lower than in the raw tracking data because errors are generally larger along the whisker shaft, where there is generally no visual cue on which to discriminate, than perpendicular to the shaft where there is usually a clear contrast between the dark line of the whisker shaft and the surrounding free space.

The estimate of 70Hz obtained for f_T is plausible as whisking itself typically ranges below 20Hz, but higher-order oscillations have been observed both in our work, and in that of other groups. The low estimates obtained for tracking errors (pixel and angle) are also plausible—the video data is of very high quality, so the bulk of these errors are likely to derive from the mouse-driven tracking interface.

Whisker curvature

Since the whisker has an inherent curvature the tracked angle will therefore differ from the angle at the base of the whisker by a small amount. Although the size of this error could be reduced by tracking the whisker closer to its base, there is a trade-off in that individual whiskers are more difficult to distinguish from their neighbors close to the mystacial pad. Knutsen et al. (2007) have recently shown that there is some torsional rotation of the whisker shaft during whisker movement, however, their

evidence also suggests that this is may be passive consequence of whisker actuation. The current analyses therefore assume that tracking errors due to whisker curvature and torsional rotation will have similar effects on all whisk types.

Measuring whisker contact

Estimates of whisker contact with the vertical surface, and of cessation of contact, were determined by frame-by-frame inspection of HSV clips. Since the overhead camera was always aligned with the vertical wall it was possible to detect contact/detach events with good accuracy, both by observing the instantaneous position of the whisker tip most proximal to the surface and by looking for bending/straightening of the whisker shaft immediately following contact/detachment. Analysis of contact judgements for three observers on 26 initial contact events showed agreement of all observers on a unique contact frame for 60% clips, and agreement to within 1 frame on 85% of clips. Mean error over all clips was 0.6 frames.

Measuring head movement

Ideally we would like to be able to measure the position and velocity of the head for all six of the available degrees of freedom (three translational, and three rotational). Unfortunately, whilst it was straightforward to extract measures of horizontal position and movement from our high-speed video (translation along two horizontal axes and rotation around the vertical axis), vertical translation and the two remaining rotations could not be obtained from the majority of clips. Of these missing measures, the most important for our analysis of whisking behavior is rotation around the coronal axis or 'head tilt', as changes in tilt can impact significantly on apparent whisker movement recorded in the overhead view. To partially address this issue, however, we were able to track the elevation of the tip of the snout in the vertical view (see, e.g. Figure S2). Snout elevation is redundantly determined by the combination of head tilt and vertical translation of the head (through, for example, crouching or rearing movements). However, since the rat's capacity for vertical translation is limited, we know that low values of snout elevation will be indicative of negative tilt (the head angled downwards to the floor), high values of positive tilt (the head angled upward towards the ceiling), and intermediate values of the head being closer to horizontal.

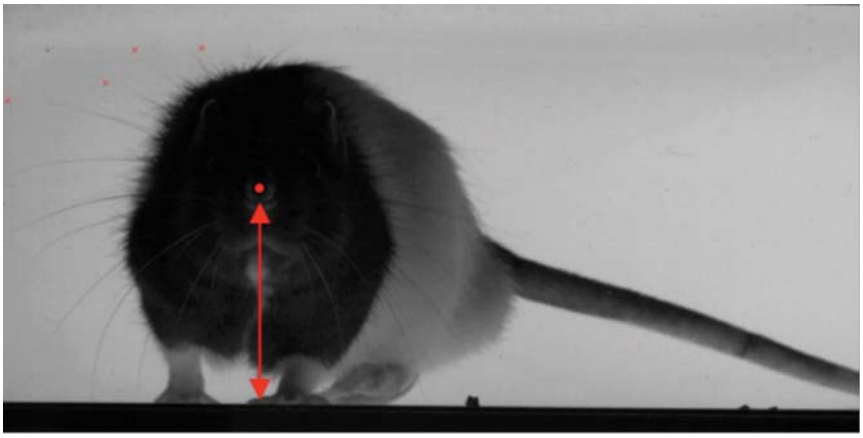

Figure S2. Snout elevation. Measured as the height of the snout tip above the floor, snout elevation provides a partial surrogate for head tilt in evaluating the effects of head-movement on observed behavior.

Partitioning clips into whisk segments

For analytical purposes it is useful to decompose each recorded bout of whisking behavior into a series of discrete episodes termed 'whisks'. A whisk is a substantial protraction of the whole whisker field followed by a retraction of similar amplitude. Whisking behavior is generally constituted of 'bouts' each consisting of a series of whisks of similar amplitudes and durations (see, e.g. Berg and Kleinfeld, 2003), however, during interactions with surfaces there may be significant variability within bouts as described in this article. Most whisks can be thought of as having two phases—a protraction phase

during which mean angular position of the whisker field is monotonically increasing, and a retraction phase during which this angle is monotonically decreasing. We can therefore define the temporal period of a whisk as the interval bounded by two successive *boundary minima* in the mean angular position. The task of partitioning trajectories is complicated, however, by the occurrence of brief reversals in the direction of whisker movement during the course of either the protraction or retraction phase. Following Towal and Hartmann (2008), such reversals, or "double pumps", are treated here as forming part of a single multi-phasic whisk rather than as creating two distinct ones. To avoid partitioning clips at these *non-boundary minima*, an initial segmentation of each whisk clip was performed by visual inspection of the clip and of the mean angular position plot. As illustrated by the exemplar raw data shown in figure 3 boundary minima can be easily distinguished from non-boundary minima when viewed within the overall context of a given whisking episode, since reversals are of smaller amplitude than the surrounding whisks in the bout. This initial segmentation identified specific time windows during which the boundary minima were considered to occur, and the precise locations of those minima were then found algorithmically by searching within these windows. Once the boundary minima were found the angle of maximum protraction, (i.e. the boundary between the protraction and retraction phases of each whisk) was determined by automated search for the maximum angular position between each successive pair of boundary minima. The search for these protraction minima and maxima always located a unique frame, in other words, there were no plateaux in the mean angular position plots within the critical time windows.

1.2 3D Whisker tip tracking and matching methods

Accuracy of whisker tip tracking

Our 3D tracking procedures required that we track the positions of the tips of the whiskers in both the overhead and side-on views. Whiskers tips were tracked manually, using a custom-built tool, in video frames displayed at pixel-for-pixel, or greater, resolution on a flat-panel LCD screen. To provide an estimate of how accurately the whiskers tips could be located using our recording apparatus, a γ macrovibrissa was mounted on a slide that was then positioned at a 45° slant in the arena so that it was visible in both camera views. An image of the slide taken from the high speed video camera was then compared with a light microscope photograph of the same slide (Figure S3). This comparison suggested that the video was of sufficient quality to allow the larger whiskers to be seen to within 1-3millimetres of the tip when stationary (93-98% of whisker length).

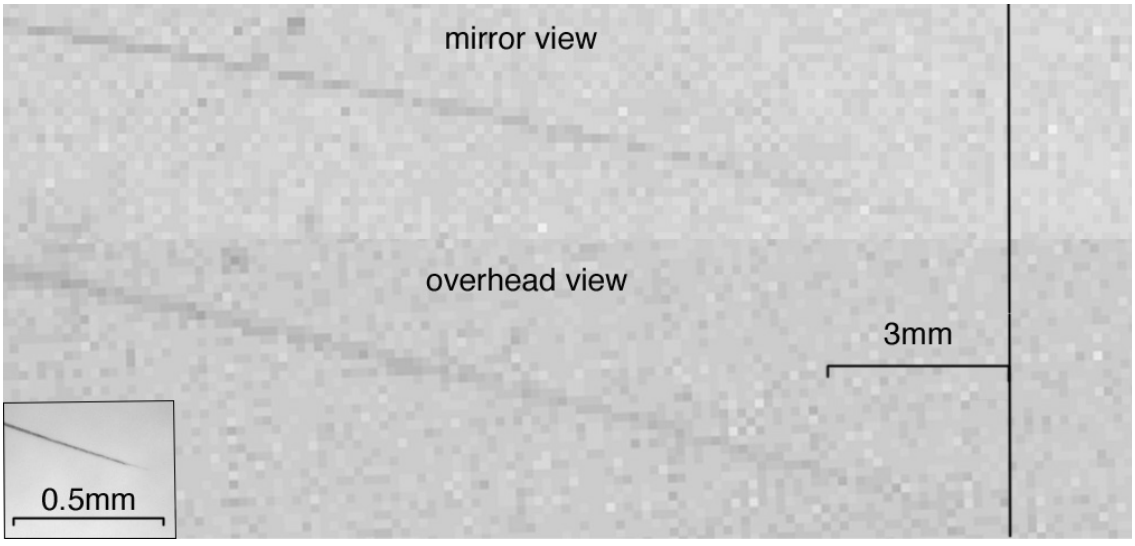

Figure S3. Mirror and overhead views of a slide-mounted macro-vibrissa. The picture is a still frame of a γ macro-vibrissa as imaged by the HSV camera. The vertical rule shows the position of the whisker tip as estimated from a light microscope photograph of the same whisker (inset). The image indicates that the tips of stationary whiskers can be detected with an accuracy of 1-3 millimetres.

Tracking whisker tips and matching using stereo correspondence

For each clip, candidate whisker-tips were labeled for tracking in the first frame of the first whisk cycle and then tracked in each frame for number of whisk cycles. The raw data generated was a number of image 'tracks' in each view that were each assumed to represent the motion of a unique whisker tip. It was assumed that at least some of the whisker tips labeled in each view were images of the same whiskers. Identifying pairs of tracks, one from each view that represented the same tips was then a matter of assessing 'stereo correspondence'. To this end, each tracked point was transformed into a line in world-space, a 'world-line', by applying the calibrated camera model in reverse (see Arena Calibration above). Thus, the tracks which were the raw data from the observer each generated a 'world-line series', with one world-line for each frame. If two points marked in the two views of a single frame are images of the same object, their world-lines are expected to approach intersection, and the point of intersection is the location of the object in 3D space. Spurious intersections are expected in single frames due to stereo ambiguity, but since the tracked objects are moving over time, these are expected to be transient. Conversely, world-line series that genuinely correspond to the same object will approximately intersect in *all* frames of a clip section. Thus, pairs of tracks that genuinely represent a single object in the world can be identified by consistently low world-line intersection error in all tracked frames (giving the motion of the tracked object over time in 3D space). The details of how these tracking and matching procedures were applied differed for the two 3D analyses described in the article as set out below.

Whisker tip trajectory reconstruction (Figure 6)

For the two clips analyzed in Figure 6 we attempted to track as many whiskers as possible on the side of the snout ipsilateral to the first surface contact. For the whisk displayed in the left-hand panel of Figure 6 an initial inspection identified 18 trackable whisker tips in the side-on view and 19 in the overhead view, for the whisk in the right-hand panel the equivalent numbers were 20 (side-on) and 14 (overhead). Tracking of each whisker tip was then performed independently by 3 observers after which a measure of inter-observer reliability e was calculated, for each whisker tip, as the average, over all tracked frames, of the distance between the individual position estimates. Whisker-tips for which $e>e(max)$, or that that were marked as untrackable in 1 or more frames by one or more observers were excluded from further analysis; for all remaining whisker-tips estimated trajectories were then calculated by averaging across observers. The 3D reconstruction algorithm subsequently found 16 (left panel) and 13 (right panel) matches between views. In both of these clips the tip of the nose and of a single ear were also tracked in both views allowing an estimate to be computed of the trajectory of the head over the course of each whisk.

Calculating a 3D measure of whisker spread (Figure S7)

For the two clips illustrated in Figure S7 our goal was not to reconstruct whisker tip trajectories *per se* but rather to calculate an estimate of whisker spread that was invariant to head movement. For this purpose 8 (S7, top panel) and 10 (S7, lower panel) whisker tips were tracked in each view by a single observer. For each possible pairing of one whisker track from each view (i.e. 64–100 possible pairings) and for each frame, an error metric was computed as the minimum Euclidean distance between the world-lines (that is, world-line intersection error). For the pairing overall, the error was recorded as the root mean square of this error over all trackable frames (using mean square emphasizes large errors in single frames, which should never arise for matched pairs). The pairing with the lowest error was then taken to be a match, the matched tracks from each view were then eliminated from the pool, and the process was repeated until no further pairings remained. With 35 whiskers per side of the face, and 8-10 whiskers tracked in each view, the expected number of matches is 2.9. This is likely to be higher in practice, however, since some whiskers are more prominent than others. We chose to take the top three matches in each of our clips, and confirmed that the errors over time in these cases were in the normal tracking error range (as determined by the more thorough trajectory reconstuction process applied to generate Figure 6). The mean 3D spread was then calculated as the mean Euclidean distances between these best three whisker matches.

1.3 Statistical considerations applied to all analyses

The primary focus of this investigation is on contrasts within triplets of consecutive whisks, data were therefore pooled across animals with the video clip of each tracked whisking episode taken as the fundamental unit for analysis. However, to guard against the possibility of Type I errors due to data pooling (Machlis et al. 1985), the main analyses were all re-computed, with animal identify as a between subject factor, and using data from just the four animals who each generated more than five eligible clips (giving 47 clips in total). Results of these analyses were consistent with those for the pooled data, in that all significant results remained significant when animal identity was included. We therefore describe here solely results for the analyses of pooled data.

Following the procedures recommended by Tabachnick and Fidell (2007) all variables were checked for outliers, normality (using the Kolmogorov Smirnov test), and sphericity (using Mauchly's test). For distributions containing outliers, relevant analyses were performed twice, with and without outliers; all such analyses were robust to this procedure and the results reported include all of the data points. Some violations of normality were detected and a number of variables were therefore log transformed to correct for positive skew. For variables that showed significant sphericity, significance values for univariate ANOVAs were calculated using the Greenhouse-Geisser correction. Post-hoc tests (Bonferroni) were used to identify the principal differences between the pre-contact, 1st contact and 2nd contact whisks. An alpha-level of 0.05 (two-tailed) was used for statistical tests corrected for multiple comparisons when required using a Bonferroni correction. Such corrections were applied whenever several univariate analyses were used to examine a specific sub-domain of active touch sensing such as whisker control, head position and movement, and whisker-surface contact. Multivariate Analysis of Variance (MANOVA) was also used to test for overall differences between whisk types in relation to each of these classes of data.

Effect sizes are reported using the partial η^2 measure. Following Cohen (1988), $0.01 < \eta^2 \leq 0.06$ can be interpreted as a small effect, $0.06 < \eta^2 \leq 0.14$ as a medium-sized effect, and $\eta^2 > 0.14$ as a large effect. In tables S1 and S2 The columns pre-contact, 1st contact, and 2nd contact show the mean and standard deviations of the relevant measure for that whisk type, and the following two columns the percentage change in the mean for the two contact whisks compared to the pre-contact value.

2 Supplementary Results

2.1 Exemplar raw data

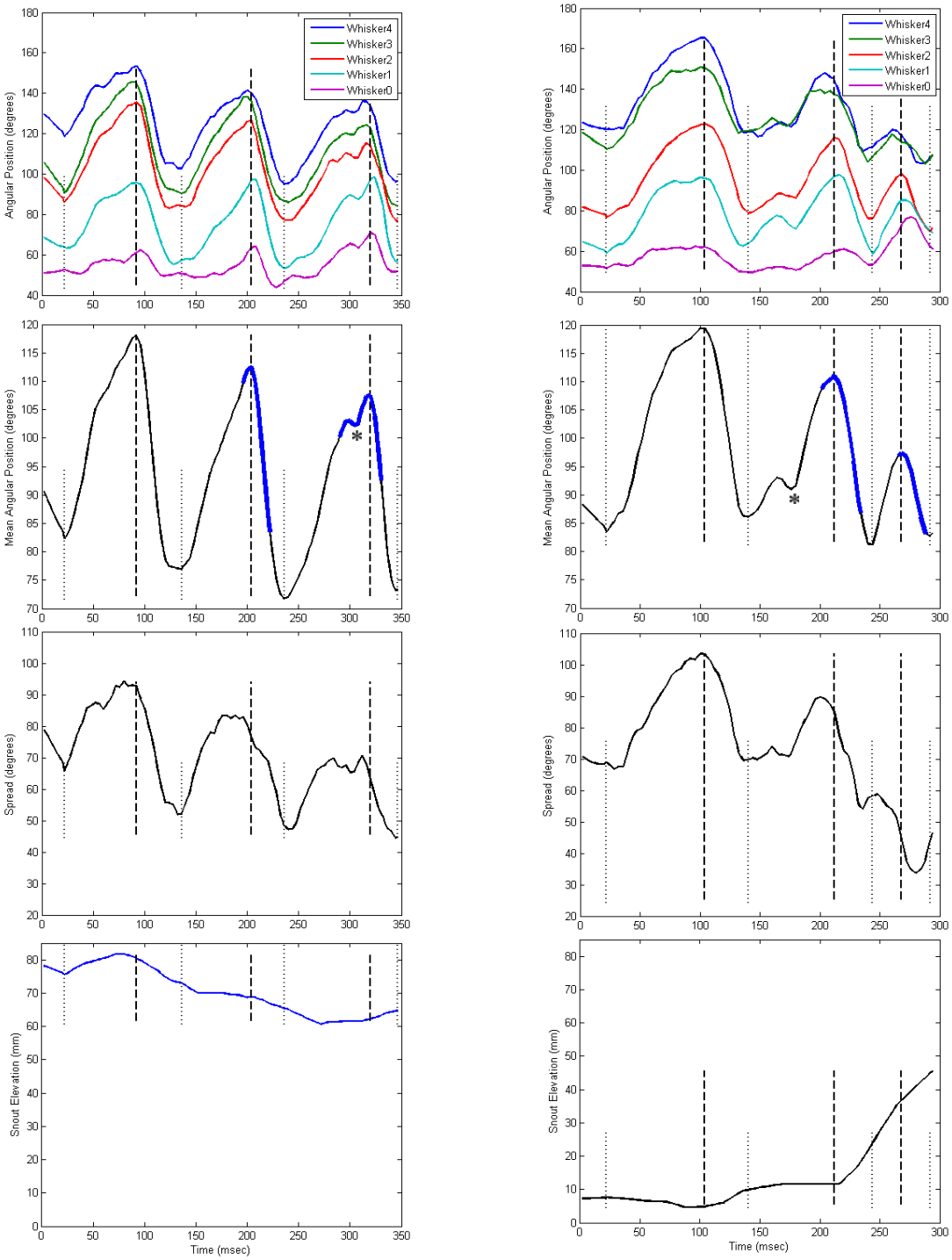

Figure S4. Exemplar raw data for two tracked video clips. From top to bottom: (i) angular position of the 5 tracked whiskers (no smoothing); (ii) mean angular position, blue overlap show periods of contact with the wall; (iii) whisker spread; (iv) snout elevation (the y-axis is based on the height of the end wall of 85mm). Dashed lines indicate the location of the boundary minima used to segment each clip into distinct whisks, dotted lines indicate the protraction maxima. Asterisks show non-boundary minima that are treated as forming part of multi-phasic whisks. The right-hand clip is the one also illustrated in Figure 4 and Supplementary Video 1.

2.3 Temporal coupling of whisker protraction and spread

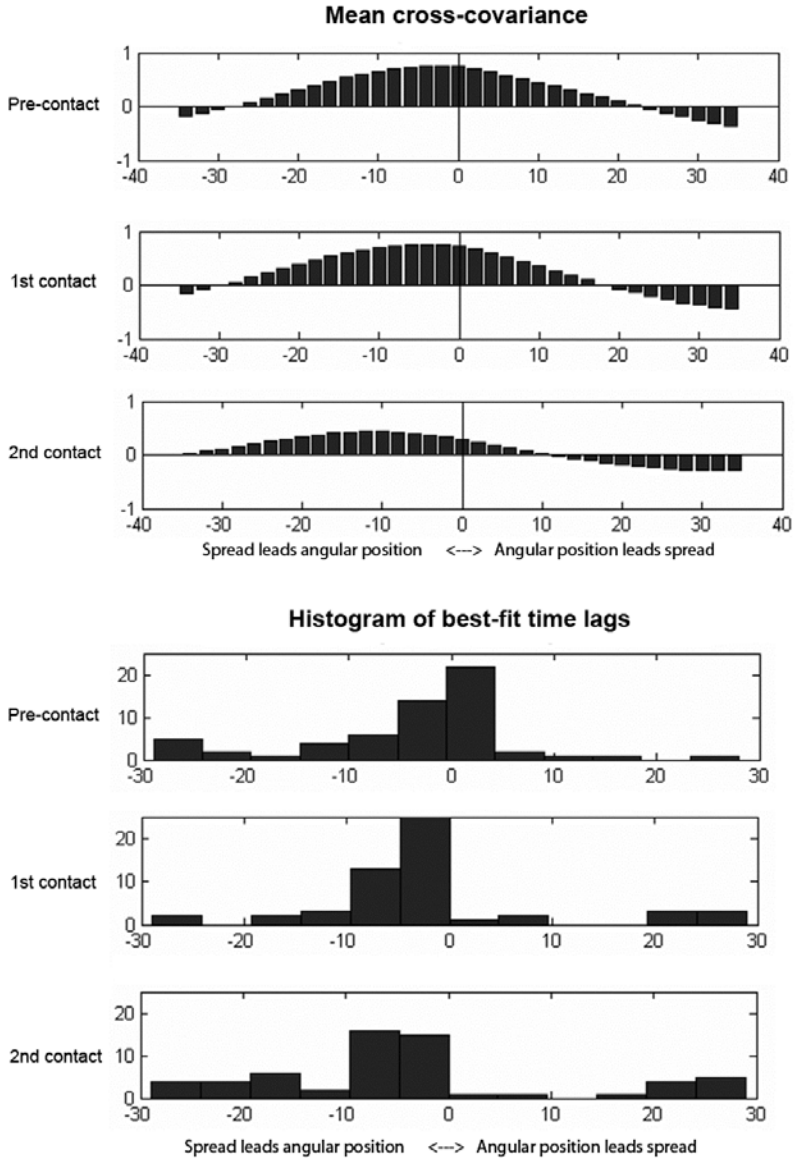

Figure S5. Differences in the temporal coupling between whisk spread and angular position. *Top:* Cross-covariance (see Chatfield, 2003) of spread and mean amplitude averaged across all 60 clips. Plots are calculated separately for each of the three whisks types: pre-contact (top), 1st contact (middle), and 2nd contact (bottom). *Bottom:* Histograms of the best-fit phase lag between spread and mean angular position, where phase lag for each whisk type in each clip is calculated as the peak of the corresponding cross-covariance plot. The coupling between spread and angular position is visibly weaker in the 2nd contact whisk. For instance in the upper half of the figure we see that the average cross-covariance has a flatter distribution and a smaller and earlier peak in the 2nd contact whisk than in either the pre-contact or 1st contact whisks, whilst in the lower half we see a more scattered distribution in the best-fit phase-lag, with out of phase relationships (more than 10ms difference between the angular position and spread peaks) in 26 (43%) of the 60 whisks.

2.4 Variation of summary measures across whisk types

Table S1. Analyses of summary whisk measures

Measure	Mean, standard dev.			% change		ANOVA			
	Pre-contact	1st Contact	2nd Contact	1st	2nd	$F_{(2,118)}$	p	Partial η^2	Post-hoc
Max. protraction (deg)	113.5, 12.0	111.1, 12.3	101.9, 13.0	-2%	-10%	41.23	<0.001[a,b]	0.411[d]	p,1>2
Min. protraction (deg)	75.5, 13.6	72.7, 10.9	70.1, 11.6	-4%	-7%	13.50	<0.001[a,b]	0.186[d]	p,1>2
Mean spread (deg)	72.2, 18.4	67.4, 19.8	57.2, 21.0	-7%	-21%	44.76	<0.001[a,b]	0.431[d]	p>1>2
Mean protraction velocity (deg/msec)	0.46, 0.20	0.44, 0.18	0.41, 0.17	-4%	-11%	1.715	0.184	0.028	n.a.
Mean retraction Velocity (deg/msec)	0.89, 0.32	0.92, 0.32	0.70, 0.35	+2%	-22%	11.33	<0.001[a]	0.161[d]	p,1>2
Whisk duration (msec)	107.3, 27.1	106.8, 25.5	98.9, 28.9	-1%	-8%	2.35	0.099	0.038	n.a.

Preliminary MANOVA showed a large multivariate difference between whisk types ($F(12,48)=7.414$, $p<0.001$, Wilks' lambda = 0.342, partial $\eta 2 = 0.650$).

a. significant using Bonferroni corrected alpha of 0.008
b. iincorporates Greenhouse-Geiser correction for non-sphericity
c. medium-size effect ($0.06 <$ partial $\eta 2 \leq 0.14$)
d. strong effect (partial $\eta 2 > 0.14$)

For post-hoc tests p= pre-contact, 1= 1st contact, 2= 2nd contact, n.a.= not applicable.

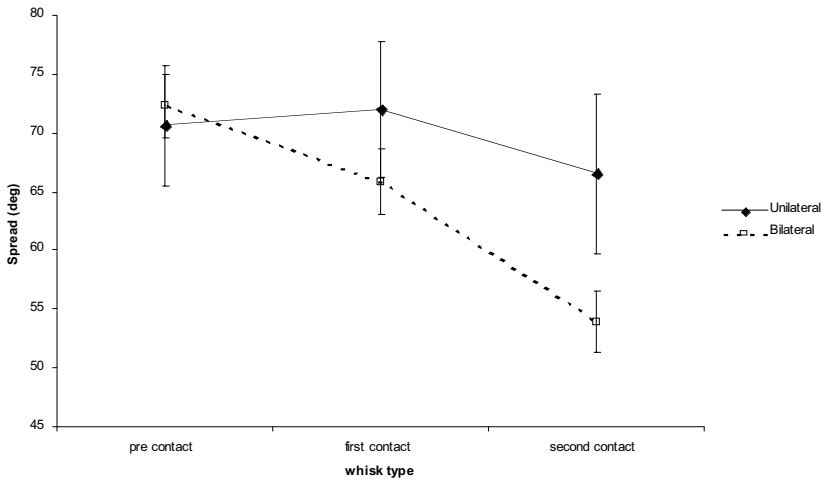

Figure S6. Change in spread across whisk types for unilateral and bilateral first contacts. 2x3 mixed ANOVA showed (i) a main effect of a significant reduction in spread ($F_{(2,116)} = 24.675$, $p<0.001$, partial $\eta^2 = 0.298$) between the 2nd contact whisk and the two previous whisks, (ii) no overall difference between bilateral and unilateral contacts ($F_{(1,58)} = 1.079$, $p=0.303$), and (iii) an interaction effect between whisk type and whether the initial contact was on one or both sides ($F_{(2,116)} = 9.423$, $p< 0.001$, partial $\eta^2 = 0.140$). This latter effect showed that the reduction in spread was more pronounced on whisks with bilateral surface contacts. Means (s.d.s) for pre-, 1st and 2nd contact whisks were unilateral 70.6 (20.3), 72.0 (23.2), 66.5 (27.4); bilateral 72.3 (17.8), 65.8 (18.4), 53.9 (17.2).

Table S2. Comparisons between 1st and 2nd Contact Whisks

Measure	Mean, standard dev.		Direction or	ANOVA		
	1st Contact	2nd Contact	% change	$F_{(1,59)}$	p	Partial η2
Number of contacts (2-5)	2.47, 0.75	2.82, 0.77	+14%	13.15	0.001[a,b]	0.182[d]
Velocity prior to contact (degrees/msec)	0.75, 0.48	0.81, 0.66	+9.0%	0.393	0.533	0.007
Mean angular position at contact (degrees)	125.1, 20.4	113.1, 19.8	-9.6%	50.27	<0.001[a]	0.460[d]
Contact duration (msec)	31.2, 14.1	43.8[e], 19.4[e]	+40.5%	13.36	0.001[a,b]	0.185[d]
Time from contact to max. protraction (msec)	14.3, 9.9	11.3, 7.0	-21.3%	4.482	0.038[b]	0.071[c]

Preliminary MANOVA showed a large difference between whisk types ($F(6,54)= 28.477$, $p<0.001$, Wilks' Lambda = 0.240, partial $\eta2 = 0.760$).

a. significant using Bonferroni corrected alpha of 0.01
b. log transformed prior to testing to correct for positive skew (Kolmogorov Smirnov test)
c. medium-size effect ($0.06 <$ partial $\eta^2 \leq 0.14$)
d. strong effect (partial $\eta^2 > 0.14$)
e. Includes clipped durations for 25 contacts that lasted beyond the end of the whisk

Table S3. Analyses of head and body movements

Measure	Mean, standard dev.			% change		ANOVA			
	Pre-contact	1st Contact	2nd Contact	1st	2nd	$F_{(2,118)}$	p	Partial η^2	Post-hoc
Distance to wall (mm)	39.2, 11.0	26.2, 9.9	17.5, 10.7	-33%	-55%	263.0	<0.001[a,b]	0.817[d]	p>1>2
Vel. to. wall (mm/msec)	0.124, 0.067	0.118, 0.067	0.057, 0.068	-4.8%	-54%	26.859	<0.001[a]	0.313[d]	p,1>2
Velocity along wall (mm/msec)	0.066, 0.045	0.079, 0.053	0.074, 0.072	+20%	+12%	0.854	0.428[b]	0.063	n.a.
Head orient. (degrees)	72.3, 22.4	74.1, 21.9	74.3, 23.4	+2.5%	+2.8%	1.64	0.199[b]	0.027	n.a
Head ang. velocity (deg/msec)	0.056, 0.062	0.059, 0.051	0.060, 0.051	+5.3%	+12.5%	0.114	0.893	0.002	n.a
Snout elev. (mm)	32.9, 29.0	31.9, 29.0	36.2, 25.7	-3%	+10%	2.23	0.112[b]	0.036	n.a.
Snout vert. velocity (mm/msec)	0.066, 0.065	0.099, 0.083	0.103, 0.109	+50%	+56%	3.992	0.021	0.063[c]	n.sig.

The columns pre-contact, 1st contact, and 2nd contact show the mean and standard deviations of the relevant measure for that whisk type, and the following two columns the percentage change in the mean for the two contact whisks compared to the pre-contact value. Preliminary MANOVA showed a strongly significant difference between whisk types ($F(12,48) = 34.828$, $p<0.001$, Wilks' Lambda = 0.086, partial $\eta2= 0.914$).

a. significant using Bonferroni corrected alpha of 0.007
b. incorporates Greenhouse-Geiser correction for non-sphericity
c. medium-size effect ($0.06 <$ partial $\eta^2 \leq 0.14$)
d. strong effect (partial $\eta^2 > 0.14$)

p= pre-contact, 1= 1st contact, 2= 2nd contact, n.a.= not applicable, n.sig= non significant.

2.3 Control analyses

Table S4. Changes in protraction velocities of most rostral and most caudal whiskers across whisk types

Measure	Mean, standard dev.			% change	
	Pre-contact	1st Contact	2nd Contact	1st	2nd
Rostral velocity	0.52, 0.31	0.53, 0.28	0.42, 0.21	+1.9%	-19.2%
Caudal velocity	0.34, 0.23	0.35, 0.19	0.42, 0.20	+2.9%	+23.5%

2x3 ANOVA: main effect of whisk type ($F_{(2, 118)}$= 0.335, p= 0.716), difference between rostral and caudal whiskers ($F_{(1, 59)}$= 24.675, p<0.001, partial η^2= 0.298), interaction ($F_{(2, 118)}$= 11.045, p<0.001, partial η^2= 0.158).

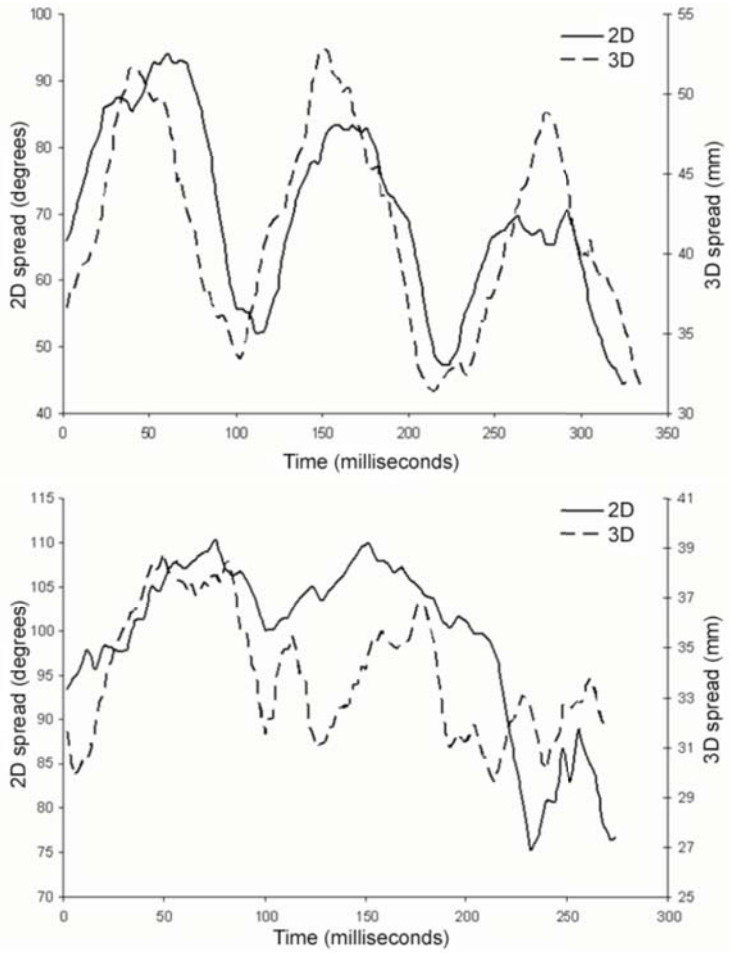

Figure S7. Comparing changes in spread as measured in two- and three- dimensions. The plots show a comparison of spread as measured in the overhead view (solid line) with the head-movement invariant measure of spread (dotted line) computed from 3D reconstruction of whisker tip trajectories for two clips. In considering this figure it is worth noting that the head-invariant measure is sensitive to changes in spread along the line of sight of the camera that are not detectable in the overhead view, thus the two traces should not be expected to be closely aligned. Nevertheless, the graphs are reasonably well correlated (r= 0.72 for the upper clip, r= 0.54 for the lower clip) and show a similar reduction in spread over the three whisk types. This comparison therefore suggests that spread, as measured in the overhead view, captures a significant portion of the variance of a measure of whisker spacing that is independent of head movement.

Table S5. Controlling for the effects of correlated control parameters on spread

Measure	Mean, standard dev.			% change		ANOVA			
	Pre-contact	1st Contact	2nd Contact	1st	2nd	$F_{(2,118)}$	p	Partial η^2	Post-hoc
Mn. spread (protraction control)	74.35, 17.35	71.08, 19.29	61.07, 20.20	-4.4%	-17.9%	35.91	<0.001[a]	0.378[d]	p,1>2
Mn. spread (contact control)	69.36, 16.36	67.22, 18.26	59.47, 19.01	-3.1%	-14.3%	15.66	<0.001[a]	0.210[d]	p,1>2
Protraction spread	72.55, 17.31	69.11, 18.44	60.68, 19.52	-4.8%	-16.4%	24.51	<0.001[a]	0.294[d]	p,1>2
Retraction spread	70.28, 20.67	60.38, 20.88	53.82 21.50	-14.1%	-23.5%	43.56	<.0001[a]	0.425 [d]	p>1>2

a. significant using Bonferroni corrected alpha of 0.0125
d. strong effect (partial $\eta^2 > 0.14$)

2.4 Sensory consequences

2.4.1 Regression analysis for the number of contacts on tracked whiskers

Potential predictors

Geometric, or head/body movement	Pearson's r	p
Distance to wall	-0.086	0.348
Inverse distance to wall	+0.104*	0.258
Head orientation	-0.107*	0.244
Snout elevation	+0.332*	<0.001
Velocity towards wall	+0.052	0.575
Whisker control		
Mean protraction velocity	-0.062	0.501
Mean retraction velocity	-0.129*	0.160
Mean spread	-0.279	0.002
Inverse mean spread†	+0.336*	<0.001

Correlations calculated for all 1st and 2nd contact whisks (n= 120)
*= selected for inclusion in regression (r>0.1)
†= Inverse mean spread has a higher correlation than mean spread (indicating that lower values of spread are more discriminative) and was therefore selected for inclusion in the regression analysis.

Final model for number of contacts

Adjusted R square= 0.136, $F_{(1,118)} = 10.388$, $p<0.001$ (using the step-wise method)

Predictor variable	β	p	Part correlation
Inverse mean spread	0.230	0.019	0.202
Snout elevation	0.222	0.024	0.195

Inverse distance to wall, head orientation, and mean retraction velocity were not significant predictors. Note that the model is a relatively week predictor explaining just 13.6% of the variance. We suspect that this is, at least in part, because of the poor resolution of the number of contacts measure which only includes contacts on tracked whiskers and thus has a range of just 2–5.

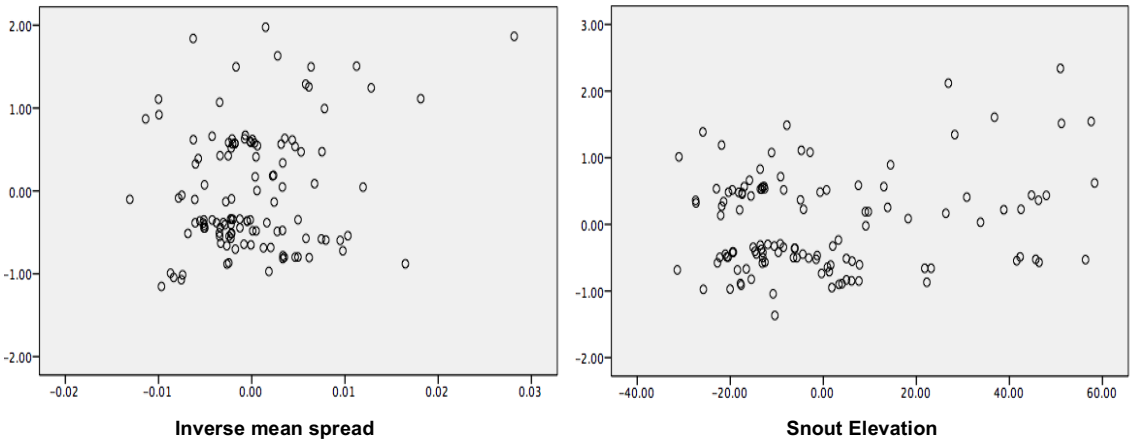

Figure S8. Residual plots for regression analysis on number of contacts. Both inverse mean spread and snout elevation show approximately linear relationships with the number of contacts, after controlling for the influence of the other predictor.

2.4.2 Additional analyses of time from contact to maximum protraction

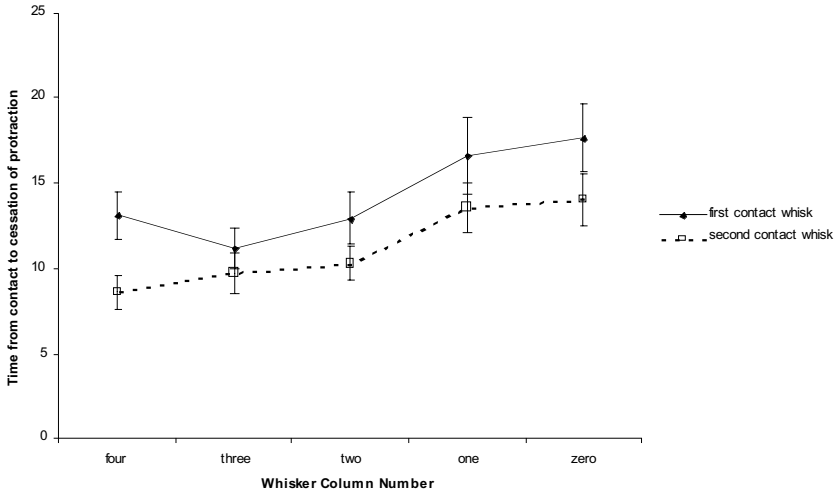

Figure S9. Mean time from contact to maximum protraction in 1st and 2nd contact whisks analysed per whisker. The mean time to maximum protraction was lower in the 2nd contact whisk across all whisker columns, suggesting a consistent effect. Retraction also began up to 5 milliseconds later in the most caudal whiskers.

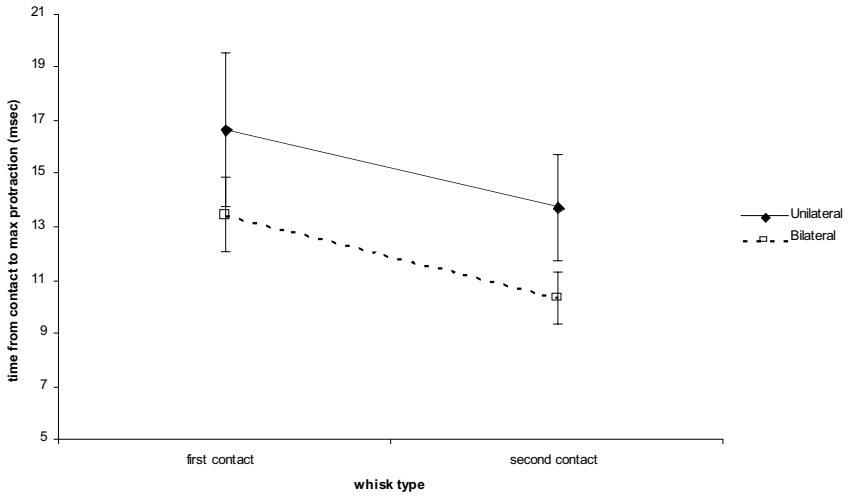

Figure S10. Mean time from contact to maximum protraction in 1st and 2nd contact whisks analysed by contact type. Cessation of protraction occurred somewhat faster in 2nd contact whisks (compared to 1st contact whisks) and following bilateral contacts (compared to unilateral contacts). A 2x2 ANOVA on this data found no main effect for whisk type ($F_{(1,58)}$ = 3.686, p=0.060) or contact type (bilateral vs. unilateral: $F_{(1,58)}$ = 2.879, p=0.095), and no interaction ($F_{(1,58)}$ = 0.003, p= 0.956). Time to maximum protraction was also compared for whisker columns that did, and did not, make contact with the wall, these were found to be very similar (F(1, 59) = 0.001, p= 0.974) indicating that the contacts themselves were not significantly distorting this measure. Means (s.d.s) for 1st, 2nd contact whisks were unilateral 16.7 (11.6), 13.7 (8.0); bilateral 13.5 (9.3), 10.4 (6.4).

2.4.3 Retraction velocity and whisk phase

Table S6. Analyses of retraction velocity for 1st (h1) and 2nd (h2) halves of the retraction phase and for the most rostral (col. 4) and most caudal (col. 0) tracked whiskers

Measure	Mean, standard dev.			% change		ANOVA			
	Pre-contact	1st Contact	2nd Contact	1st	2nd	$F_{(2,118)}$	p	Partial η^2	Post-hoc
Overall mean (Table 2)	0.89, 0.32	0.92, 0.32	0.70, 0.35	+2%	-22%	11.33	<0.001[a]	0.161[d]	p,1>2
H1 mean	1.05, 0.48	0.92, 0.48	0.48, 0.35	-12%	-54%	46.013	<0.001[a]	0.438[d]	P,1>2
H2 mean	0.86, 0.43	0.92, 0.41	0.78, 0.48	+7%	-9%	1.458	0.237	0.024	n.a.
Col. 4 H1 (rostral)	1.171, 0.643	1.086, 0.592,	0.622, 0.466	+6%	-47%	25.173	<0.001[a]	0.303[d]	p,1>2
Col. 0 H1 (caudal)	0.646, 0.453	0.448, 0.389	0.329, 0.333	-30%	-49%	10.764	<0.001[a]	0.157[d]	p>1,2

a. significant using Bonferroni corrected alpha of 0.0125
b. incorporates Greenhouse-Geiser correction for non-sphericity
c. medium-size effect ($0.06 < \text{partial } \eta^2 \leq 0.14$)
d. strong effect (partial $\eta^2 > 0.14$)

For post-hoc tests p= pre-contact, 1= 1st contact, 2= 2nd contact, n.a.= not applicable

2.4.4 Regression analysis for contact duration

Potential predictors for contact duration

Head position and movement	Pearson's r	p
Distance to wall	-0.051	0.622
Inverse distance to wall	+0.014	0.898
Head orientation	-0.031	0.768
Snout elevation	+0.145*	0.161
Angle of whisker contact with wall	-0.118*	0.256
Velocity towards wall	-0.227*	0.027
Snout vertical velocity	-0.299*	0.003
Whisker control		
Mean protraction velocity	-0.267*	0.009
Mean retraction velocity	-0.261*	0.011
Time from contact to max protraction	+0.477*	<0.001

Correlations calculated for all 1st contact whisks and 35 2nd contact whisks (n= 95)
*= selected for inclusion in regression (r>0.1)

Final model

Adjusted R square= 0.391, $F_{(1,118)} = 16.072$, p<0.001 (using the step-wise method)

Predictor variable	β	p	Part correlation
Time from contact to max. protraction	0.498	<0.001	0.487
Mean retraction velocity	-0.298	<0.001	-0.293
Snout vertical velocity	-0.250	0.003	-0.246
Snout elevation	0.187	0.025	0.183

Velocity towards wall, angle of whisker contact, and mean protraction velocity were not significant predictors.

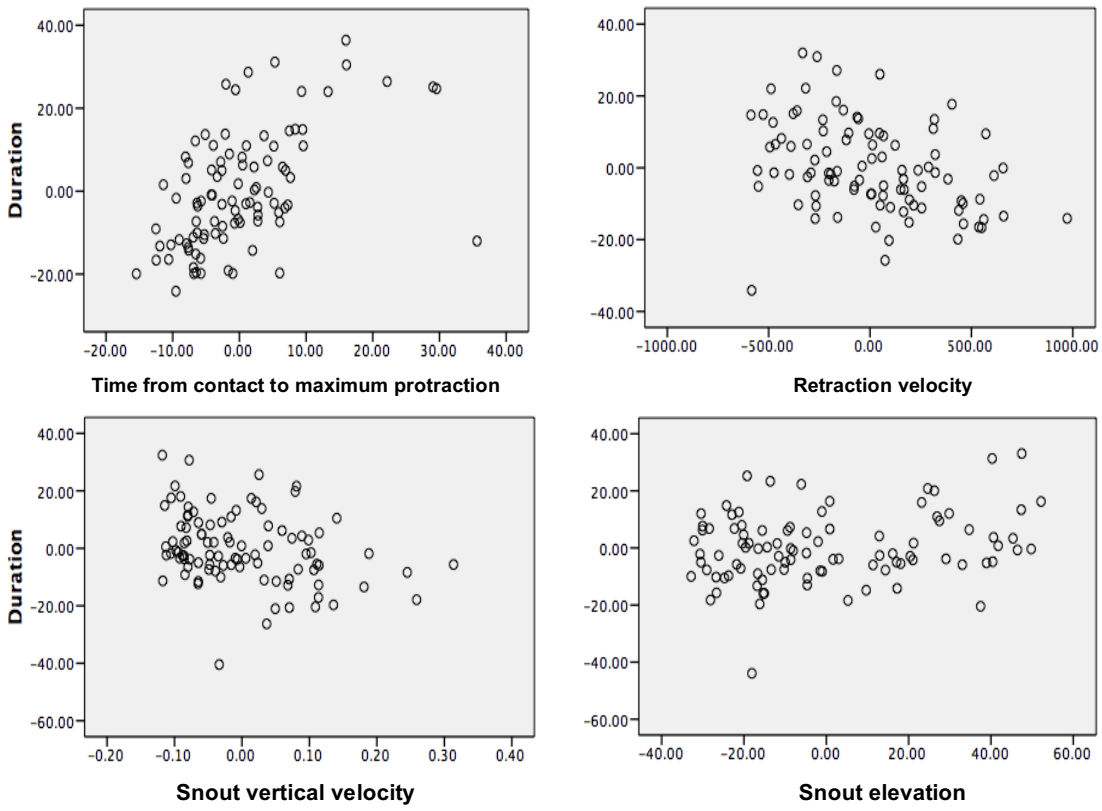

Figure S11. Residual plots for regression analysis of contact duration. Both time from contact to maximum protraction and retraction velocity show approximately linear relationships with the contact duration after controlling for the influence of other predictors.

3 References used in this supplement

Berg RW, and Kleinfeld D. Rhythmic whisking by rat: retraction as well as protraction of the vibrissae is under active muscular control. *J Neurophysiol* 89: 104-117, 2003.

Chatfield C. *The Analysis of Time Series: An Introduction*. London: Chapman and Hall, 2003.

Cohen J. *Statistical power analysis for the behavioral sciences*. Hillsdale, NJ: Lawrence Earlbaum Associates., 1988.

Knutsen PM, Biess A, and Ahissar E. Vibrissal kinematics in 3D: tight coupling of azimuth, elevation, and torsion across different whisking modes. *Neuron* 59: 35-42, 2008.

Machlis L, Dodd PWD, and Fentress JC. The pooling fallacy: problems arising when individuals contribute more than one observation to the data set. *Zeitschrift fu¨r Tierpsychologie* 68: 201–214, 1985.

Tabachnick BG, and Fidell LS. *Using Multivariate Statistics*. Boston: Pearson International, 2007.

Towal RB, and Hartmann MJ. Variability in velocity profiles during free air whisking behavior of unrestrained rats. *J Neurophysiol* 2008.

Tsai RY. (1987) "A versatile camera calibration technique for high-accuracy 3D machine vision metrology using off-the-shelf TV cameras and lenses,'' *IEEE Journal of Robotics and Automation*, Vol. RA–3, No. 4, August 1987, pp. 323–344.